EVALUATION OF ONE-DIMENSIONAL SITE RESPONSE IN CALIFORNIA DOWNHOLE ARRAYS

Ramin Motamed[1], Gangjin Li[1], and Stephen Dickenson[2]

[1] Department of Civil & Environmental Engineering, University of Nevada Reno, Reno
[2] New Albion Geotechnical, Inc., Reno

Abstract

This paper presents the one-dimensional (1D) site response analysis (SRA) of three geotechnical downhole arrays in California subjected to both strong and weak earthquake shakings. The arrays were initially assessed in terms of effectiveness of 1D SRA using taxonomy exercise. Then SRA were performed utilizing finite element program LS-DYNA to study the site effects of the selected arrays. Lastly, the predictions were compared with the recorded counterparts and the uncertainties of the 1D SRA models were evaluated. Among the analyzed ground motions, we focus on the analysis results of the mainshock and aftershock of 2014 M_w 6.0 South Napa Earthquake.

Introduction

The 2014 M_w 6.0 South Napa Earthquake caused the strongest shaking in much of the Northern San Francisco Bay region since the 1989 M_w 6.9 Loma Prieta earthquake. During this event, 14 geotechnical downhole arrays of California Strong Motion Instrumentaion Program (CSMIP) recorded ground-motion data (Shakal et al., 2014), which are available for download at the Center for Engineering Strong Motion Data (CESMD) website (*http://www.strongmotioncenter.org/*). These recordings have been examined by many researchers to understand the propagation of the seismic waves (Bray et al., 2014, Celebi et al., 2015).

This study investigates the influence of local site effects on the amplification of seismic motions in three CSMIP geotechnical downhole arrays with records of significantly high peak ground accelerations (PGA) during the South Napa Earthquake. Taxonomy evaluation of the arrays was carried out to provide implications for 1D SRA on a priori basis. Furthermore, LS-DYNA, an advanced Finite Element (FE) program, was utilized to develop 1D SRA models for these arrays in order to evaluate the influence of the 1-D approximations on computed site response: (1) all boundaries are horizontal and extend infinitely, and (2) the response is dominated by vertically propagating and horizontally polarized shear (SH) waves. Both strong and weak shaking motions were used to perform SRA for each downhole array. And the analysis results were compared with the observations at every available downhole sensor depth in order to examine the effectiveness of SRA models in capturing soil response. On the basis of the analyses performed to date, the practical limitations of 1D site response analysis for the selected arrays have been identified and discussed in this paper.

Selection of Geotechnical Downhole Arrays

Array Selection Criteria

Considering the fourteen CSMIP geotechnical downhole arrays that recorded motions during the 2014 M_w 6.0 South Napa Earthquake, we carried out a screening procedure to select a few arrays of interest that meet the following criteria:

1. Accelerometers measure bi-directional shaking (i.e. two horizontal components);
2. The array has recorded both small and moderate-to-large amplitude motions (PGA < 0.1 g and PGA > 0.15 g);
3. Recorded ground motions are regarded as free-field motions and are not affected by an adjacent structure;
4. The soil layers are not susceptible to liquefaction and liquefaction has not previously been observed at close proximity to the array;
5. The site geology is relatively simple and a soil column can reasonably represent the subsurface soil behavior (i.e. minor basin or topography effects);
6. Arrays with information on subsurface soil properties such as in-situ test data.

Selected Arrays

Ideally, the candidate arrays meet all the criteria as listed above; however, it is acknowledged that site-specific aspects of the local geology, topography, and level of site characterization will diverge from these criteria to some extent. In most cases, the constraints have to be relaxed for selecting sites. In this study, we eventually identified 3 vertical arrays including (1) Crockett - Carquinez Bridge Geotech Array #1 (CC #1), (2) Crockett – Carquinez Bridge Geotech Array #2 (CC #2), (3) Vallejo - Hwy 37/Napa River E Geo. Array (Vallejo). All these arrays are located to the south of Napa Valley in Northern California. The local geology is complex with the bedrock consisting of interbedded marine claystone, siltstone, and fine-grained sandstone of the Late Cretaceous Panoche Formation. Boreholes were drilled at the selected sites and shear wave velocity (V_s) and compression wave velocity (V_p) were measured using PS suspension logging by California Department of Transportation (Caltrans). The site characteristics of the selected arrays are summarized in Table 1. It is noteworthy that the ground water table (GWT) depth of all three sites are shallow, generally less than 14 ft, but there was no evidence of liquefaction during the South Napa earthquake, and application of liquefaction screening and triggering evaluation procedures indicates that the soils had a very low susceptibility for generation of significant excess pore pressure during the South Napa earthquake. It was determined that all 3 of the selected arrays are located in close proximity to structures (i.e. bridges), therefore the recorded ground motions were examined for evidence of soil-structure interaction.

Crockett - Carquinez Bridge Geotech Arrays #1 & #2

Crockett – Carquinez Bridge Geotech arrays #1 and #2 are located close to the south anchorage structure of the westbound Alfred Zampa suspension bridge and eastbound cantilever truss bridge on Interstate 80 over the Carquinez Strait. At the south end of the suspension bridge,

Table 1. Site characteristics of selected arrays (CESMD, *www.strongmotioncenter.org)*

Station No.	Station Name	Site Geology	Sensor Depths (m)	$V_{s,30}$ (m/sec)	z_{1000} *(m)	Site Class (ASCE 7-10)	GWT Depth ** (m)	Distance to Adjacent Structure (m)
68206	Crockett - Carquinez Br #1	Shallow clay over rock	0, 20.4, 45.7	345	>46	D	4	~10
68259	Crockett - Carquinez Br #2	Shallow clay over soft rock	0, 61, 125	173	>125	D	0.9	0
68310	Vallejo - Hwy 37/Napa River E	Bay mud	0, 17.9, 44.5	509	>35	C	3	~70

Note: (1) Z_{1000}: the depth where V_s reaches 1000m/sec; (2) GWT depth is estimated as the depth where V_p reaches 1500m/sec.

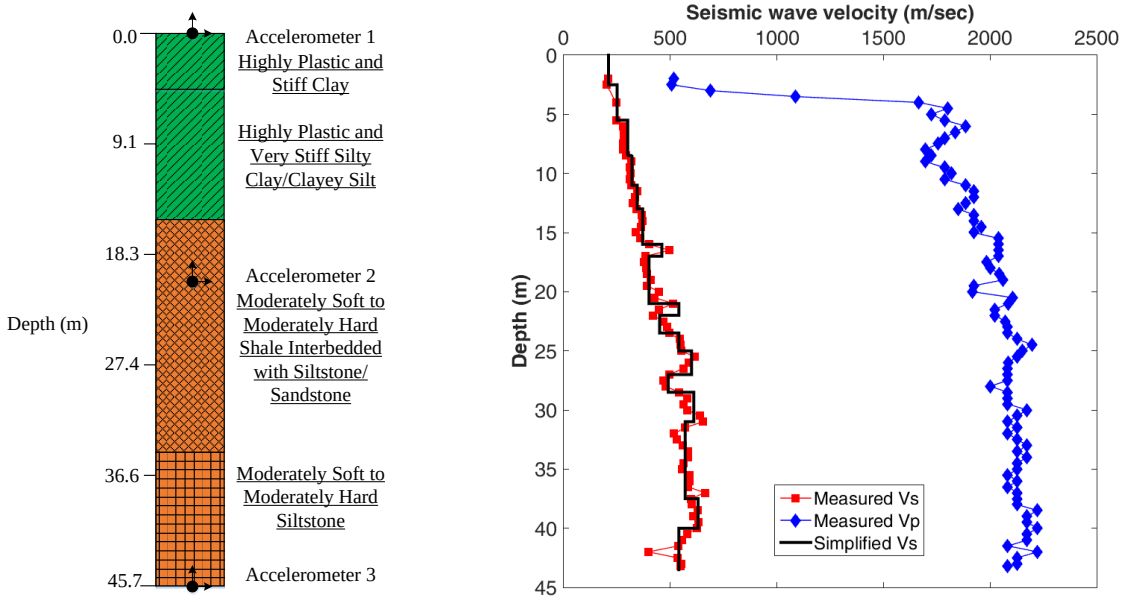

(a) (b)

Figure 1. (a) Geologic section (personal communication with Caltrans) and (b) seismic wave velocity profile of CC #1 (adopted from CESMD, *www.strongmotioncenter.org*)

the site consists primarily of up to 15 feet of fill underlain by soft to stiff clay (about 5-15 feet thick) which is much like young Bay Mud. Below this bay mud is very stiff clay (about 15-30 feet) containing weathered rock fragments. Below the very stiff clay is the bedrock consisting of

interbedded siltstone, claystone and shale with closely spaced factures. Figures 1 and 2 present the soil, V_s and V_p profiles of CC #1 and 2.

Downhole sensors were installed for both CC #1 and CC #2 at three depths (0 m, 20.4 m, 45.7 m for CC #1 and 0 m, 61 m, 125 m for CC #2). In addition, CC #1 is outside the bridge roadways and ramps and is not as close to the bridge ramp as is CC #2. CC #2 is deployed between several bents of the roadway south of the bridge crossing and the Crockett off-ramp. Although they are located nearby each other (roughly 200 m away), the site characteristics of CC #2 are different from CC #1. Compared to CC #1, the site of CC #2 is softer with a deeper bedrock.

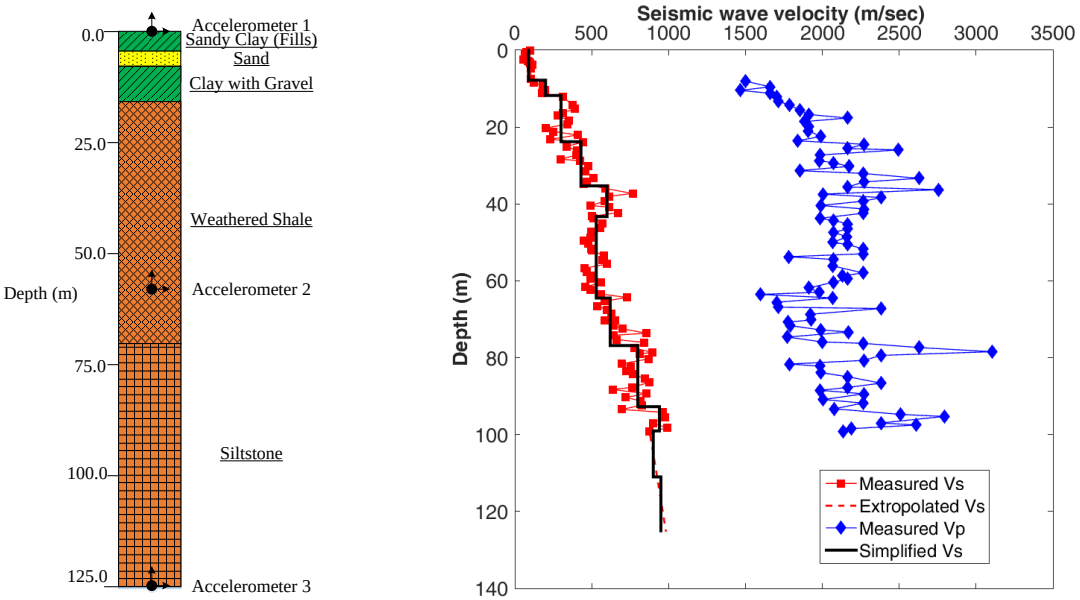

(a) (b)

Figure 2. (a) Geologic section (personal communication with Caltrans) and (b) seismic wave velocity profile of CC #2 (adopted from CESMD, *www.strongmotioncenter.org*)

Vallejo – Hwy 37/Napa River E Geo. Array

Vallejo array is located adjacent to the east abutment of the Hwy37/Napa River Bridge with three downhole accelerometers at depths of 0 m, 17.9 m and 44.5 m. The site is consisted of stiff clay layer underlain by silty clay. Beneath the silty clay is weathered fractured sandstone. The geologic section and seismic wave velocity profile of this array are presented in Figure 3.

Taxonomy Evaluation of Selected Arrays

The site classification scheme (i.e. taxonomy) proposed by Thompson et al. (2012) was employed to quantify site response complexity and assess the validity of the 1D site response assumptions for the selected downhole arrays.

The sites have been separated into four distinct categories, i.e. LG, LP, HP and HG sites, based on the classification scheme of Thompson et al. (2012). The first letter of the taxonomy

notation indicates the inter-event variability (σ) class of empirical transfer functions (ETFs) (H for "high" and L for "low") while the second letter indicates the goodness-of-fit (r) between ETFs and theoretical transfer functions (TTFs) (G for "good" and P for "poor"). The threshold values of σ and r are 0.35 and 0.6, respectively. In order to minimize the potential for nonlinear effects and increase the statistical significance, Thompson et al. (2012) recommended to use at least 10 records with PGA < 0.1g at ground surface for taxonomy evaluation.

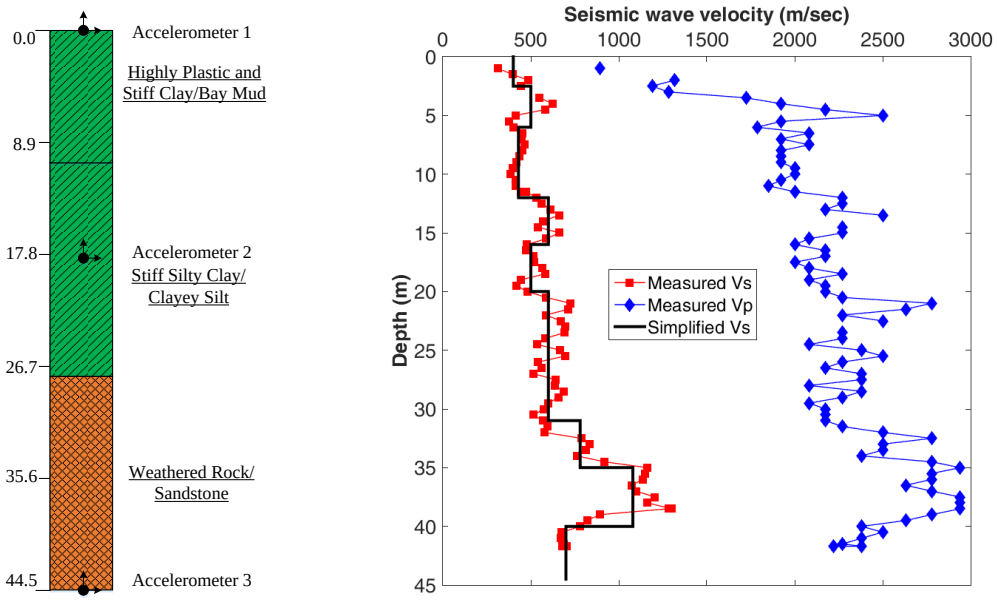

(a) (b)

Figure 3. (a) Geologic section (personal communication with Caltrans) and (b) seismic wave velocity profile of Vallejo (adopted from CESMD, *www.strongmotioncenter.org*)

As illustrated in Figures 4, 5 and 6, we evaluated the taxonomy for each selected downhole array by using the weak ground shaking (PGA at surface instrument < 0.1g) from the CESMD website (*http://www.strongmotioncenter.org/*) and the associated FTP folder containing a database of low-amplitude motions (PGA < 0.5% g) for vertical arrays and surface free-field sites. The number of "linear" motions utilized are 21, 15 and 18 for CC #1, CC #2 and Vallejo, respectively. ETFs were calculated as the ratio of Fourier spectra amplitude between the surficial and deepest accelerometers as given in Eq. (1) (Afshari et al., 2015). The ETF is taken as the geometric-mean of ETFs for the two horizontal components of the recordings (at their as-recorded azimuths) for each site. On the other hand, TTFs were computed according to the viscoelastic theory of Kramer (1996) for multi-layered and damped soil profiles implemented in Matlab (Mathworks, 2015).

$$H(f) = \frac{G(f,x_1)}{G(f,x_2)} \quad (1)$$

where $G(f,x_1)$ and $G(f,x_2)$ are amplitude spectra at surface and the deepest downhole sensor, and $H(f)$ is the ETF.

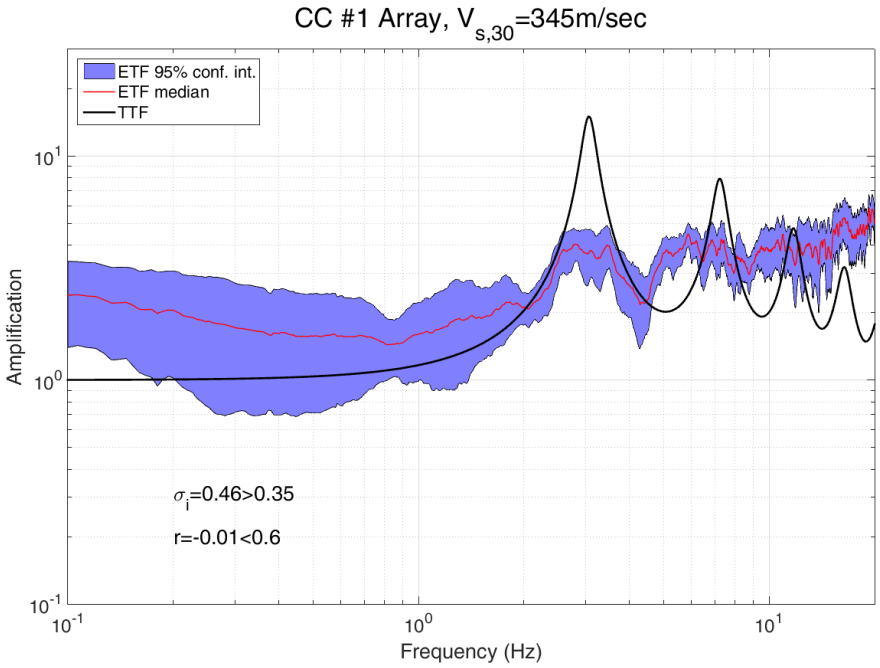

Figure 4. Taxonomy evaluation of CC #1

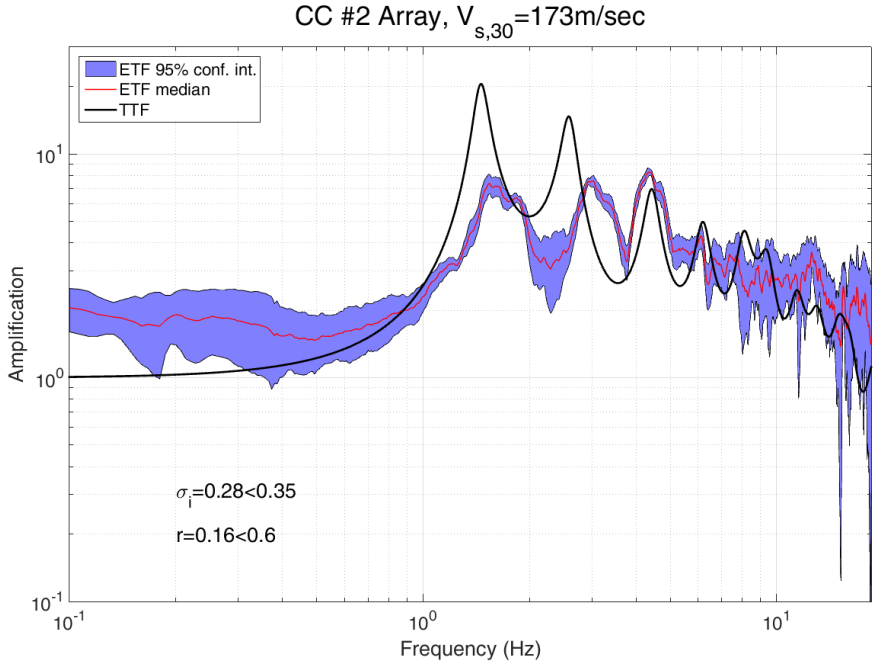

Figure 5. Taxonomy evaluation of CC #2

According to the results presented in Figures 4 to 6, it was found out CC #1 can be classified as a HP site, which means it was not informative for nonlinear constitutive models

unless path and source effects can be accounted for (Thompson et al., 2012). Besides, CC #2 and Vallejo are grouped into LP sites indicating that they are appropriate for nonlinear modeling but care must be taken to identify the source of misfit (Thompson et al., 2012).

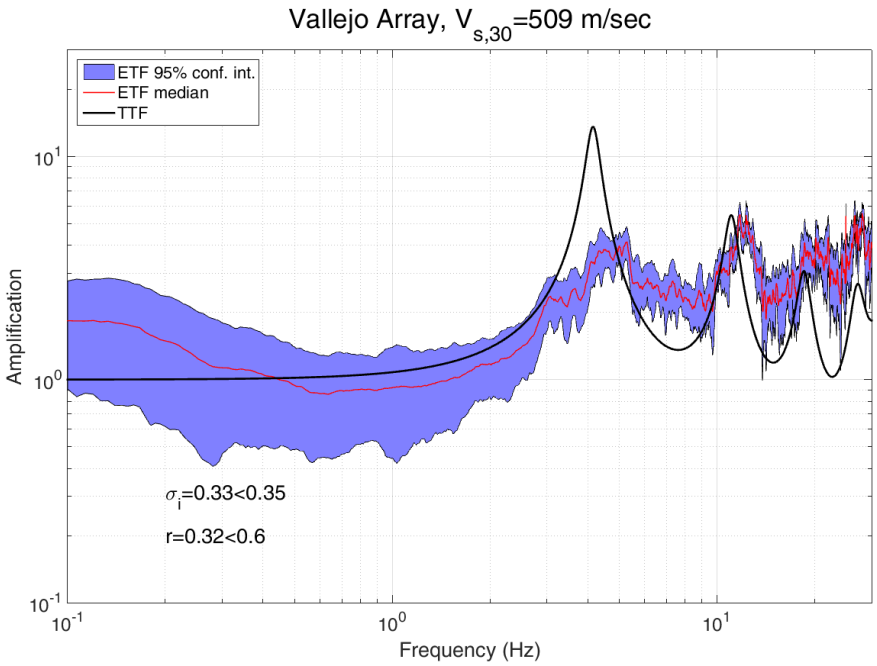

Figure 6. Taxonomy evaluation of Vallejo

1D Site Response Analysis

Methodology

Three bi-directional 1D site response analysis models were developed for CC #1, CC #2 and Vallejo using LS-DYNA (LSTC, 2012). The constraints of 1-D modeling are acknowledged; soil layer boundaries are horizontal and extend infinitely in lateral directions and seismic waves propagate vertically (SH waves). Single soil column models, (Figure 7), were developed for the selected arrays in LS-DYNA using solid elements constrained to move in shear. The soil columns were discretized in such a way that the maximum frequency each layer could propagate was as close to 37.5 Hz as possible. The bases of the soil columns were fixed to represent the "within" profiles (Stewart et al., 2008). In current engineering practice soil deposits are routinely modeled with lumped mass, springs and dampers for 1D SRA (e.g., DeepSoil, Hashash et al., 2016). Alternatively, SRA modeling with advanced FE programs such as LS-DYNA may be advantageous in some situations as they can take the effect of multi-directional shaking into account. In this study, the recorded acceleration data at the deepest downhole sensors of each array were input in both horizontal directions (bi-directional shaking) simultaneously to study the interaction between the horizontal components of the site response.

The influence of dynamic stress-strain behavior on computed site response were investigated using three different soil backbone models, including general quadratic/hyperbolic

backbone curve (Groholski et al., 2016, denoted as GQH hereafter) , modified two-staged hyperbolic backbone curve (Motamed et al., 2016, denoted as MTH hereafter) and linear elastic curve (denoted as L hereafter). For all three models, small strain damping (D_{min}) was applied using the DAMPING_FREQUENCY_RANGE_DEFORM feature in LS-DYNA which provides approximately frequency-independent damping over a range of frequencies to element deformation. D_{min} was set as 2% and 5% for strong and weak shakings in the frequency range of 1~30 Hz, respectively.

Regarding the nonlinear soil models including GQH and MTH, MAT_HYSTERETIC_SOIL model was employed to simulate the dynamic response of the soil deposit, which includes an option to adjust soil stiffness based on the level of strain rate. Dynamic soil behavior was characterized by modified two-stage hyperbolic backbone curve for MTH model and general bivariate quadratic equation for GQH model. These two models were developed to properly account for the maximum shear stress in the constitutive model at large strain. Hysteretic damping of soil materials is governed by the loading-unloading relationship as described by Masing rule (Masing, 1926). Rate-dependent effects of clayey soils were accounted for by applying a 5% increase in stiffness per log cycle of plastic strain rate.

With respect to linear soil model, which assumes the stress-strain response of the soil is viscoelastic and viscous damping ratio is independent of strain and frequency, the linear elastic material was defined by MAT_ELASTIC command. At all strain levels, the viscoelastic formulation uses the small-strain, linear-elastic shear modulus (G_{max}).

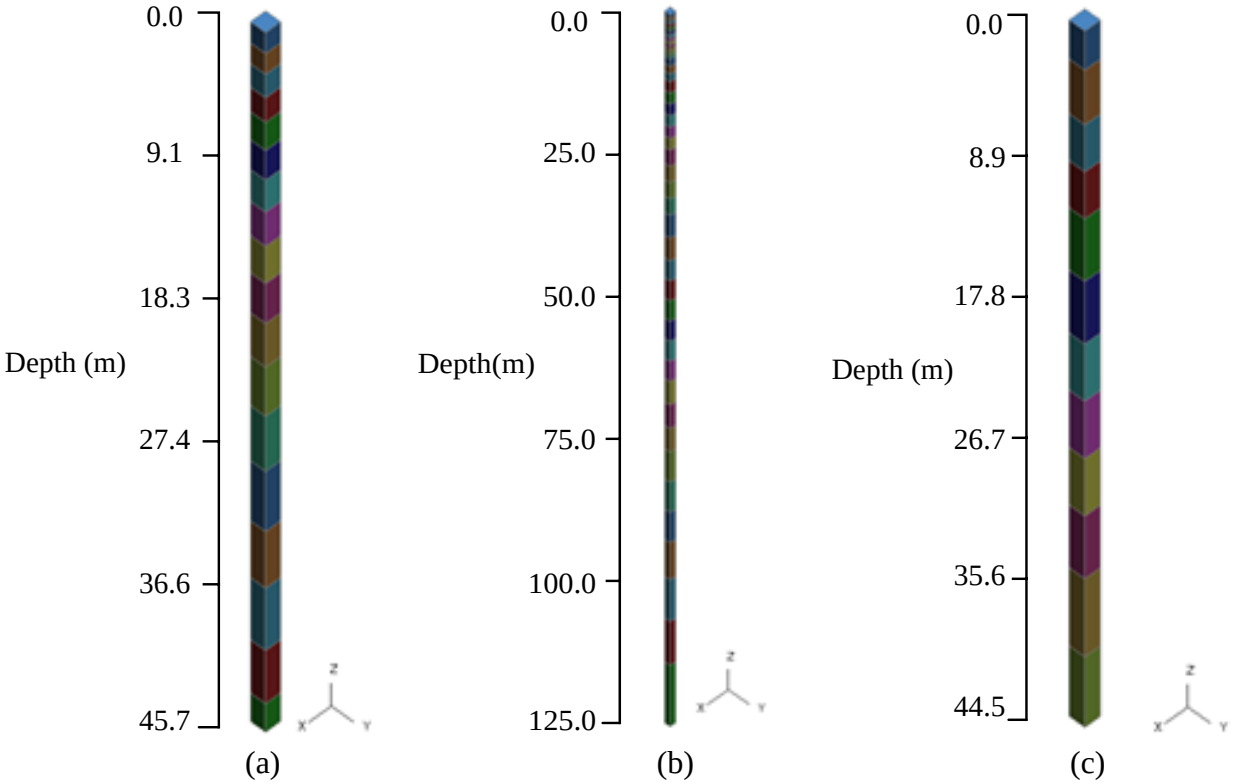

Figure 7. LS-DYNA soil column models for (a) CC #1 (b) CC #2 and (c) Vallejo

Selection of Ground Motions

For each selected downhole array, six individual analyses were performed including one strong shaking case (the mainshock of South Napa Earthquake) and five weak shaking cases (including two aftershocks of South Napa Earthquake, an M_w 3.6 on August 24, 2014 and an M_w 3.9 on August 26, 2014). The processed ground motion time series were downloaded through the CESMD website (*http://www.strongmotioncenter.org/*). The number of records of the three downhole arrays is plotted against PGA level at ground surface ($PGA_{surface}$) in Figure 9. As can be seen from this figure, the majority of the records has relatively small amplitudes (< 0.1 g). Several motions with $PGA_{surface}$ greater than 0.1 g were observed during the South Napa Earthquake mainshock. Specifically, CC #1 with the nearest rupture distance (R_{rup}) of 20.0 km recorded the largest PGA where the north-south (NS) component reached approximately 1.0 g while CC #2 recorded a much smaller PGA of 0.44 g. Also at Vallejo, with R_{rup} of 11.4 km, recorded a PGA of 0.198 g in east-west (EW) direction.

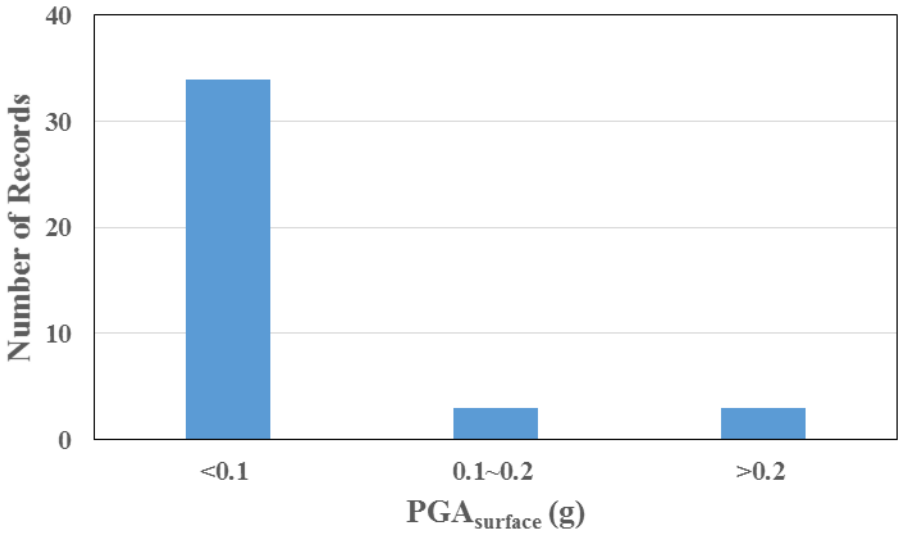

Figure 8. Number of records per PGA level at ground surface in studied arrays

Analysis Results and Discussions

This section discusses the 1D site response analysis results of the selected downhole arrays subjected to the mainshock (M_w 6.0, 2014/08/24) and aftershock (M_w 3.9, 2014/08/26) of South Napa Earthquake.

CC #1, South Napa Earthquake Mainshock

By comparing the recordings of both surficial and downhole sensors in Figure 9, it is observed that the ground motions were similar between depths of 20.4 m to 45.7 m for CC #1. The higher frequency motions were significantly amplified when propagating from the depth of 20.4 m to the surface at CC #1.

It is shown in Figures 9 and 10(a) that the spectral acceleration (Sa) and PGA predictions of GQH and MTH models reach fairly good agreement with the observations at mid-depth of

20.4 m. However, these two backbone models underpredicted spectral acceleration at period less than 0.4 sec and PGA at surface. In contrast, linear elastic model overpredicted the soil response at 20.4 m depth while it surprisingly performed much better in capturing the large amplification at surface, especially in the EW direction. The nonlinear soil behavior was not dominant in the soil profile as shown in Figure 10(b) with peak shear strain smaller than 0.1%.

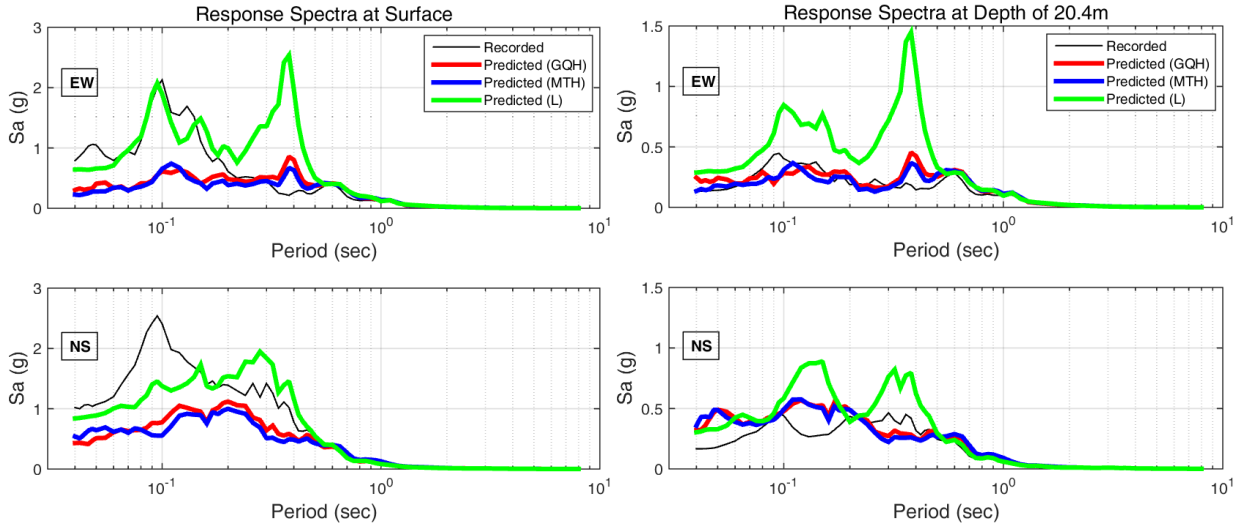

(a) (b)

Figure 9. Comparison of measured and predicted spectral acceleration of CC #1 under the shaking of South Napa Earthquake mainshock at (a) surface and (b) 20.4 m depth

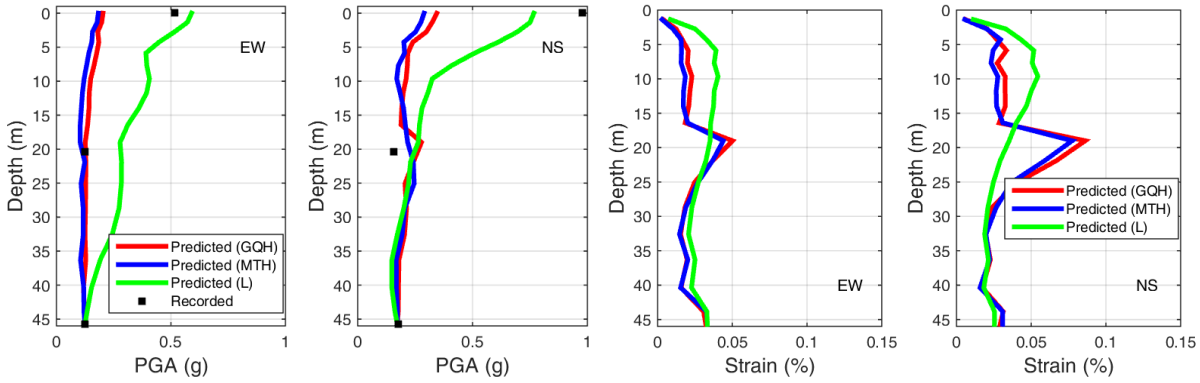

(a) (b)

Figure 10. (a) PGA and (b) max shear strain profiles of CC #1 under the shaking of South Napa Earthquake mainshock

Residuals of acceleration response spectra were computed based on the definition of Stewart et al. (2008) as shown in Eq. 2.

$$R(T) = \ln(S_a(T))_{data} - \ln(S_a(T))_{pre} \quad (2)$$

Where $\ln(S_a(T))_{data}$ is the spectra of recordings and $\ln(S_a(T))_{pre}$ is the spectra of model predictions. The positive residual indicates underprediction while negative residual implies overprediction of the model.

As shown in Figure 11(a), both linear and nonlinear models exhibited quite large residuals at the surface throughout a wide period range. This observation confirmed the taxonomy of CC #1 (HP site) which implied the site tended to yield poor fits for 1D SRA.

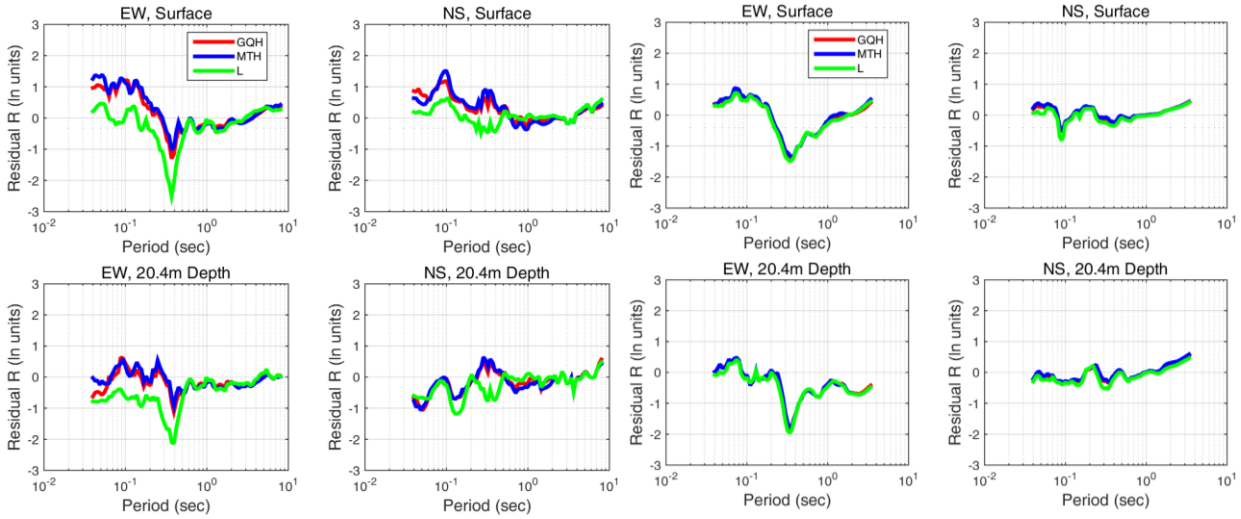

(a) (b)

Figure 11. Spectral acceleration residuals of CC #1 under the shaking of (a) South Napa Earthquake mainshock and (b) South Napa Earthquake aftershock

CC #1, South Napa Earthquake Aftershock (08/26/2016)

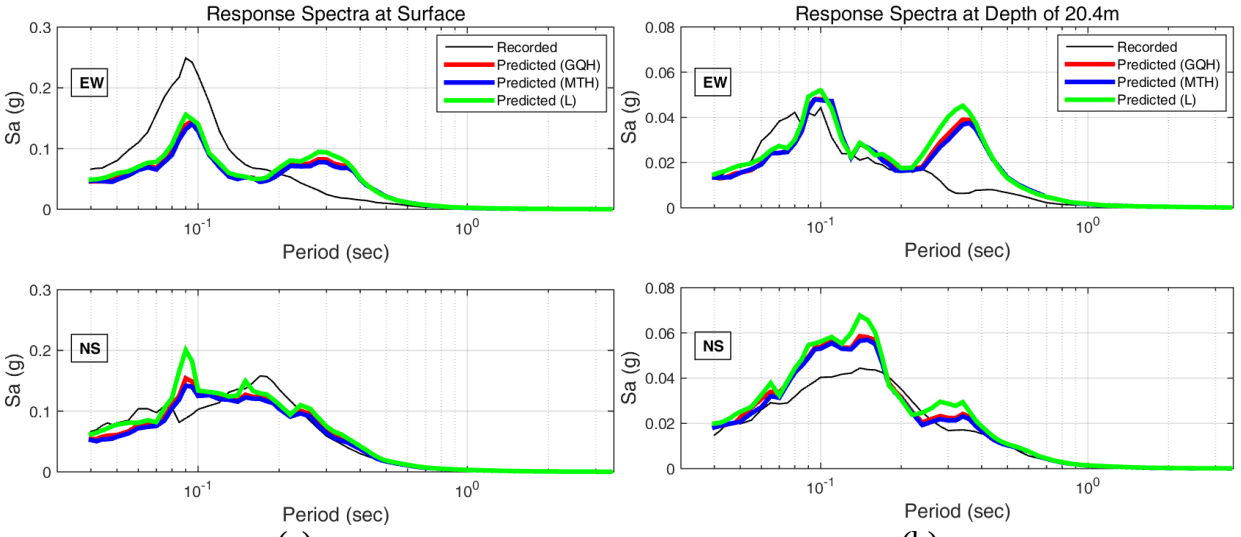

(a) (b)

Figure 12. Comparison of measured and predicted spectral acceleration of CC #1 under the shaking of South Napa Earthquake aftershock at (a) surface and (b) 20.4 m depth

As can be observed in Figures 12 and 13(a), both nonlinear (GQH and MTH) and linear models agreed well with the recorded data at 20.4 m depth (EW and NS components) and surface (only NS component). Nevertheless, all models failed to reproduce the soil response at

surface in the EW direction. Additionally, the soil behaved elastically, which was confirmed by the very similar results produced by both nonlinear and linear models, with peak shear strain smaller than 0.003% as shown in Figure 13(b).

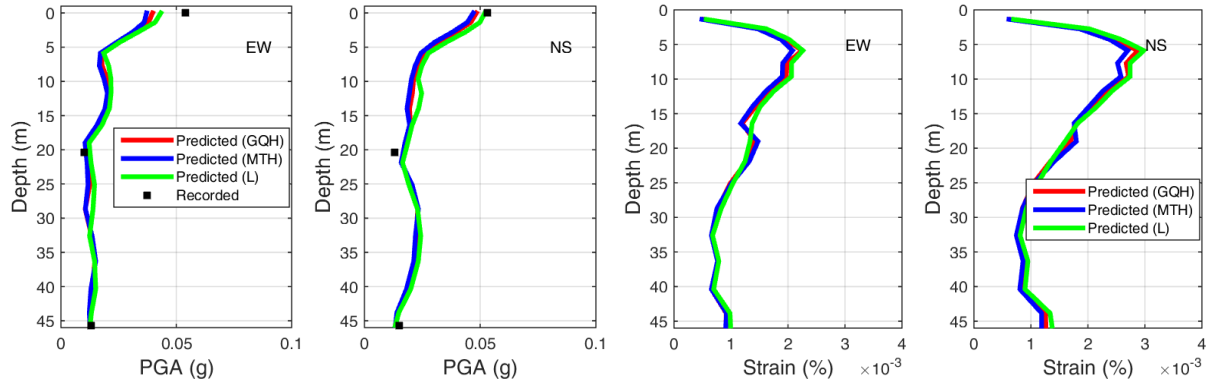

Figure 13. (a) PGA and (b) max shear strain profiles of CC #1 under the shaking of South Napa Earthquake aftershock

Overall, the residuals of the aftershock (weak event) decreased at every depth and both directions in comparison with the counterparts of the mainshock (strong event) as shown in Figure 11(b). The improved performance of nonlinear models at this weak shaking case with very small strain confirmed the taxonomy class of CC #1 (HP) suggesting this site is not suitable for calibrating nonlinear 1D SRA to recorded motions.

CC #2, South Napa Earthquake Mainshock

Similar to CC #1, at CC #2, the ground motions exhibited large amplifications from the mid-depth sensor (61 m) to the surficial sensor as presented in Figure 14. Very minor to negligible amplification was noted at depths between 61 m and 125 m for CC #2.

Figures 14 and 15(a) demonstrates good comparison was achieved for GQH and MTH models with regard to spectral acceleration and PGA in the EW direction at surface and in the NS direction at mid-depth of 61 m. However, they slightly underestimated spectral acceleration and PGA at surface (NS component) and overestimated spectral acceleration and PGA at 61 m depth (EW component). Conversely, general overestimation was noticed at all depths (EW and NS components) for linear elastic model. Figure 15(b) shows the shear strain level in the soil profile reached as high as about 0.4% indicating the soil behavior entered nonlinear stage under this strong shaking.

As illustrated in Figure 16(a), the spectral acceleration residuals of all models approach to 0 at periods longer than about 0.7 sec. The overall performance of nonlinear models with smaller spectral acceleration residuals is significantly better than linear model. These observations reflect that CC #2 is appropriate for calibrating nonlinear SRA as indicated by its taxonomy evaluation (LP site).

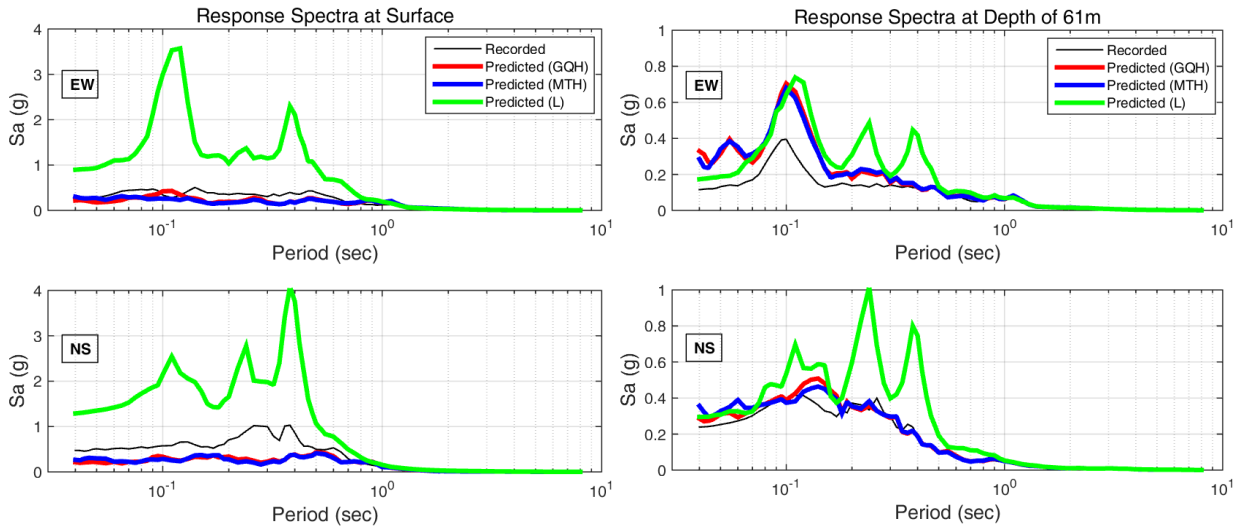

(a) (b)

Figure 14. Comparison of measured and predicted Sa of CC #2 under the shaking of South Napa Earthquake mainshock (a) surface and (b) 61 m depth

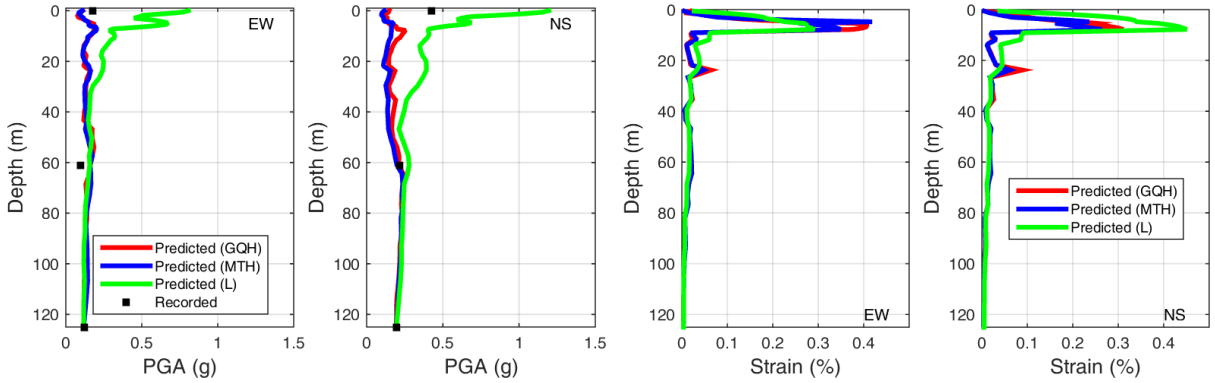

(a) (b)

Figure 15. (a) PGA and (b) max shear strain profiles of CC #2 under the shaking of South Napa Earthquake mainshock

CC #2, South Napa Earthquake Aftershock (08/26/2016)

Figures 17 and 18(a) illustrate the three models (GQH, MTH and L) in general captured the soil response at different depths in both EW and NS directions. The mobilized shear strain level (about 0.01%) as shown in Figure 18(b) is much higher than CC #1 (about 0.003%) although the PGA at CC #1 is larger when subjected to the same event. This is due to the fact that the site of CC #2 is softer than CC #1 as shown in Figures 1 and 2.

As demonstrated in Figure 16(b), all spectral acceleration residuals of linear elastic model are much closer to nonlinear models under the weak shaking compared to the counterparts under the strong shaking. The performance of linear model is improved for this event since the soils behaved essentially linearly and the induced shear strain level was very low.

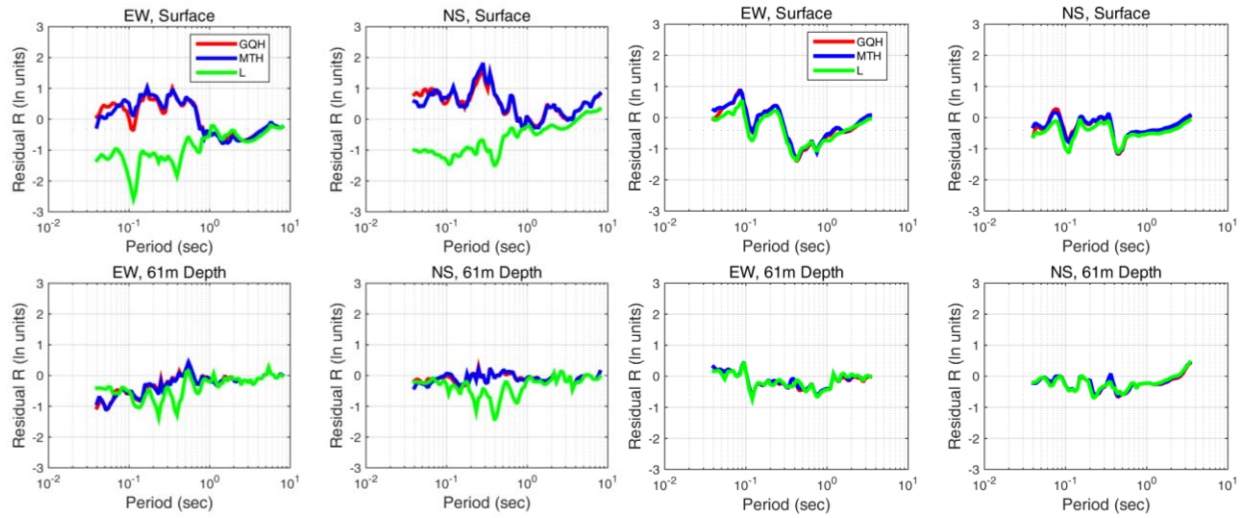

(a) (b)

Figure 16. Spectral acceleration residuals of CC #2 under the shaking of (a) South Napa Earthquake mainshock and (b) South Napa Earthquake aftershock

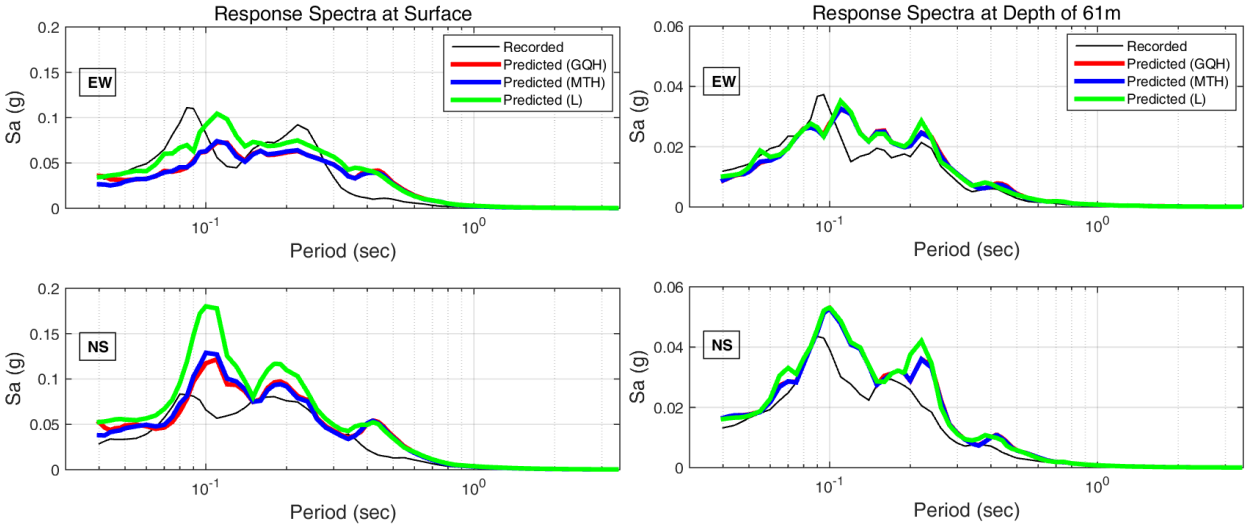

(a) (b)

Figure 17. Comparison of measured and predicted spectral acceleration of CC #2 under the shaking of South Napa Earthquake aftershock (a) surface and (b) 61 m depth

Vallejo, South Napa Earthquake Mainshock

The predictions of GQH and MTH models are in reasonable agreement with the recorded motions in the EW direction at surface and 17.9 m depth in terms of spectral acceleration and PGA as presented in Figures 19 and 20(a). Nevertheless, they in general overestimated the soil response in the NS direction at both depths, especially around 0.3 sec. In addition, the linear elastic model exhibited overestimation in both EW and NS directions at all depths. The maximum shear strain was roughly 0.05% as shown in Figure 20(b), which indicates the nonlinearity is not prevailing in the soil profile.

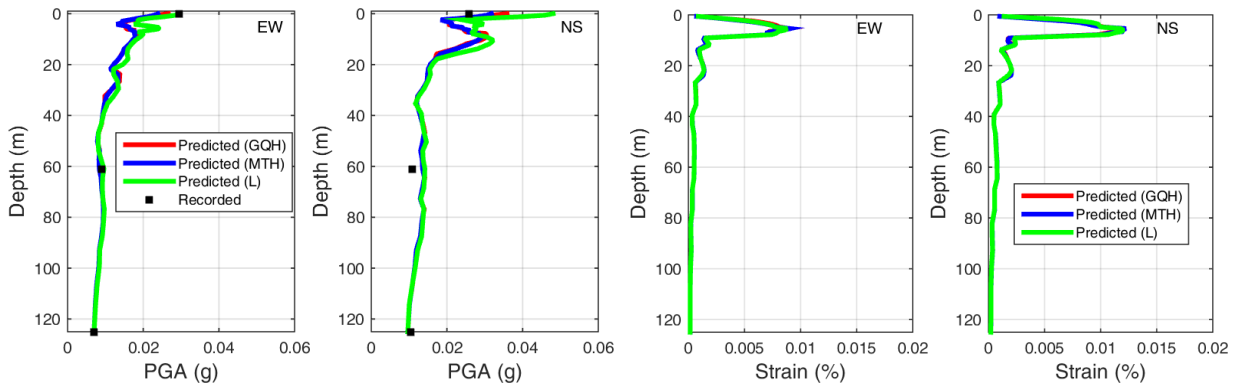

(a) (b)

Figure 18. (a) PGA and (b) max shear strain profiles of CC #2 under the shaking of South Napa Earthquake aftershock

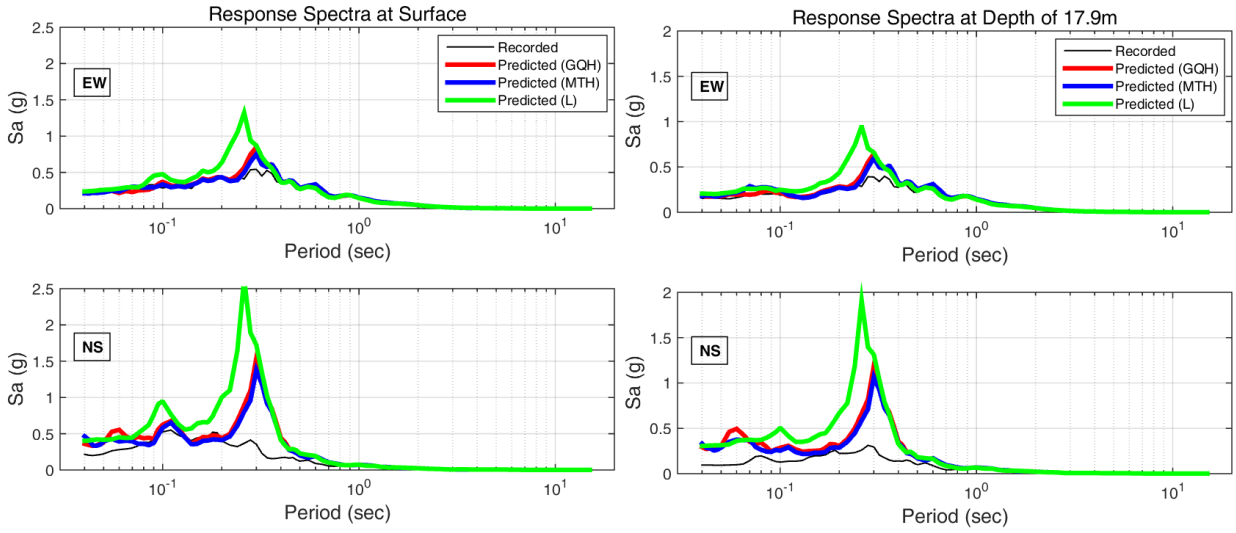

(a) (b)

Figure 19. Comparison of measured and predicted spectral acceleration of Vallejo under the shaking of South Napa Earthquake mainshock (a) surface and (b) 17.9 m depth

As presented in Figure 21, the spectral acceleration residuals are very close to 0 except the NS components at periods smaller than 1.0 sec. This observation is consistent with its taxonomy evaluation (i.e., LP site) demonstrating that Vallejo is ideal for calibration of nonlinear SRA.

Vallejo, South Napa Earthquake Aftershock (08/26/2016)

As can be observed in Figures 22 and 23(a), all three models fairly well reproduced the soil response for all components at various depths. However, remarkable overestimation occurred around 0.25 sec for NS components at surface and 17.9 m depth. The soil behavior remained elastic with peak shear strain approximately 0.001% as shown in Figure 23(b).

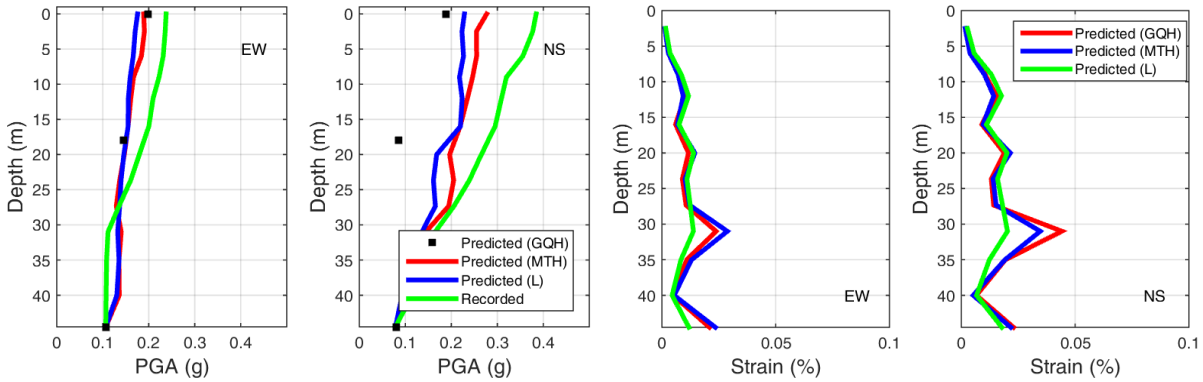

Figure 20. (a) PGA and (b) max shear strain profiles of Vallejo under the shaking of South Napa Earthquake mainshock

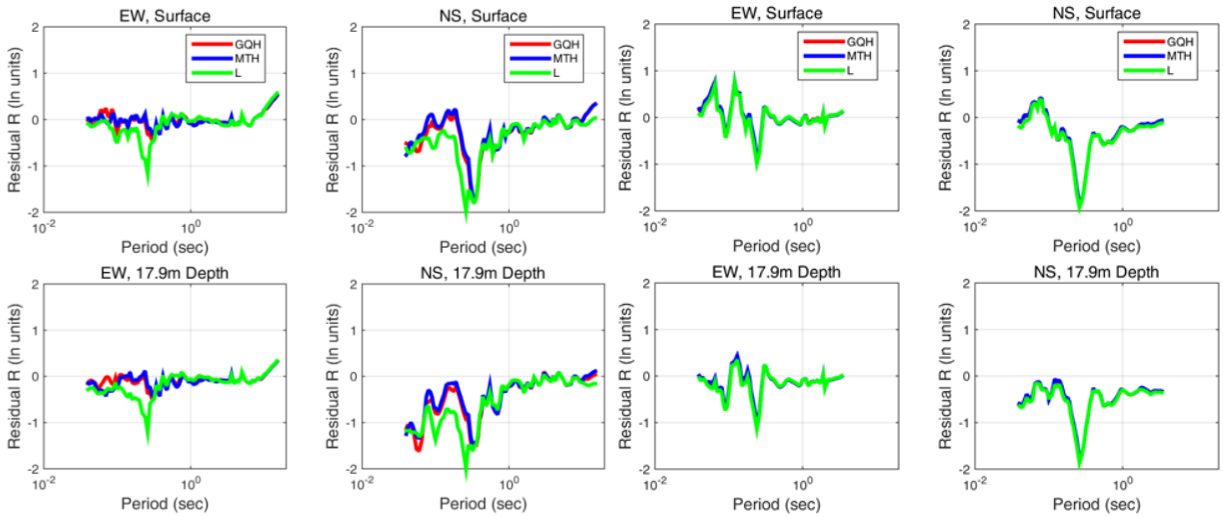

Figure 21. Spectral acceleration residuals of Vallejo under the shaking of (a) South Napa Earthquake mainshock and (b) South Napa Earthquake aftershock

As illustrated in Figure 21(b), the spectral acceleration residuals of all three models are almost identical with each other. In general, the spectral acceleration residuals are negative at surface (NS direction) as well as at 17.9m depth (EW and NS directions). Additionally, spectral acceleration residuals are generally positive at periods smaller than about 0.6 sec and get closer to 0 when periods increase in the EW direction at surface.

Correlation of Taxonomy with Spectral Acceleration Residuals

Figure 24 presents a summary plot to correlate taxonomy designations with surface spectral acceleration residuals of MTH models for CC #1, CC #2 and Vallejo under both strong shaking (the South Napa mainshock) and weak shaking (the South Napa aftershock). Geometric mean was used to combine the two orthogonal horizontal components of ground motion. And the residuals were computed as the average values over short period range (< 0.5 sec) and long

period range (> 0.5 sec). Each subplot is divided by dashed red lines into four panes representing the taxonomy class the sites fall into. Besides, the size of the circles in Figure 24 is linearly proportional to the magnitude of the residuals. The texts adjacent to the circles indicate the actual values of residuals.

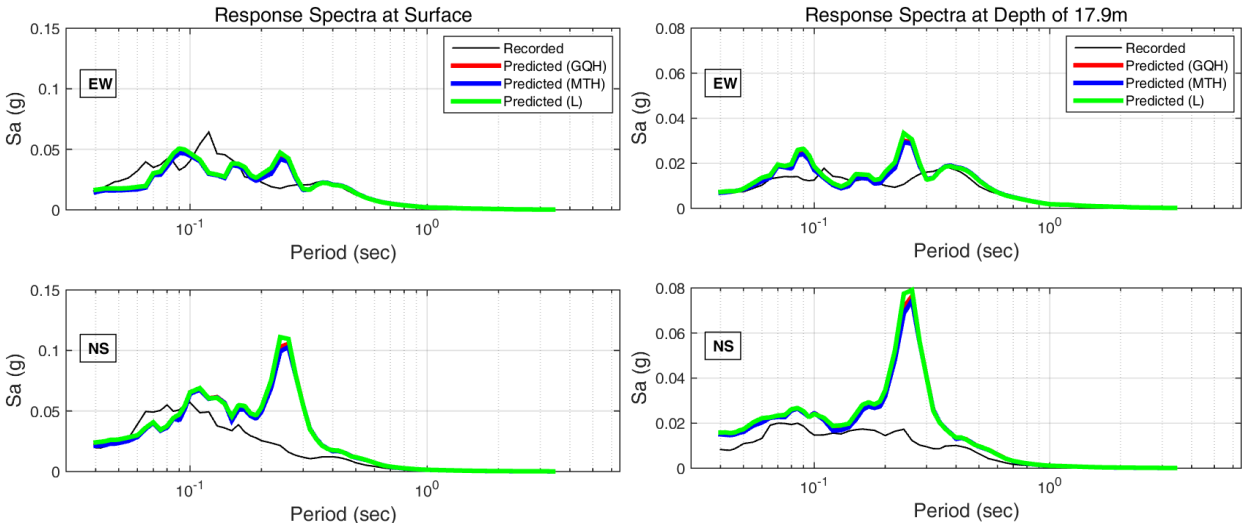

(a) (b)

Figure 22. Comparison of measured and predicted spectral acceleration of Vallejo under the shaking of South Napa Earthquake aftershock (a) surface and (b) 17.9 m depth

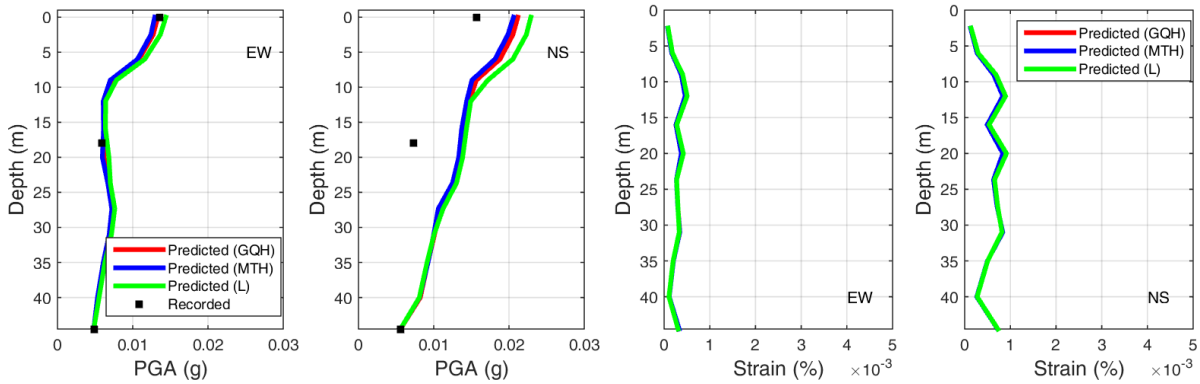

(a) (b)

Figure 23. (a) PGA and (b) max shear strain profiles of Vallejo under the shaking of South Napa Earthquake aftershock

In general, the residuals are larger in magnitude at short period range than at long period range for all arrays and both shaking cases. This means the MTH models were better in reproducing the low frequency contents of the ground motions.

Also, Figure 24 illustrates CC #1 has much larger residuals in magnitude under strong shaking than under weak shaking regardless of period range (0.63 vs. 0.01 throughout short period range and 0.16 vs. 0.01 throughout long period range). This agrees with the indication of taxonomy class of CC #1 as a HP site that it is not a good site for calibrating nonlinear constitutive models.

As implied by taxonomy scheme, Vallejo is a LP site and thus could be well characterized by nonlinear soil models. It is shown in Figure 24 that the residuals of Vallejo are very comparable when subjected to strong and weak shakings at the same period range. This observation is consistent with the implication of taxonomy evaluation.

Similar to Vallejo, the taxonomy class (LP) of CC #2 can be confirmed by the smaller residual of long period range in strong shaking case compared to weak shaking case. However, it is surprising that the residual of short period range is significantly larger in magnitude than the counterpart of long period range. This may be caused by topography effects or soil-structure interaction effects. It is noteworthy that CC #2 has overall higher residuals in magnitude than Vallejo given the same period range and the same shaking case. This can explained by the fact that the goodness-of-fit correlation coefficient of CC #2 is lower than that of Vallejo although these two arrays are both grouped into LP sites.

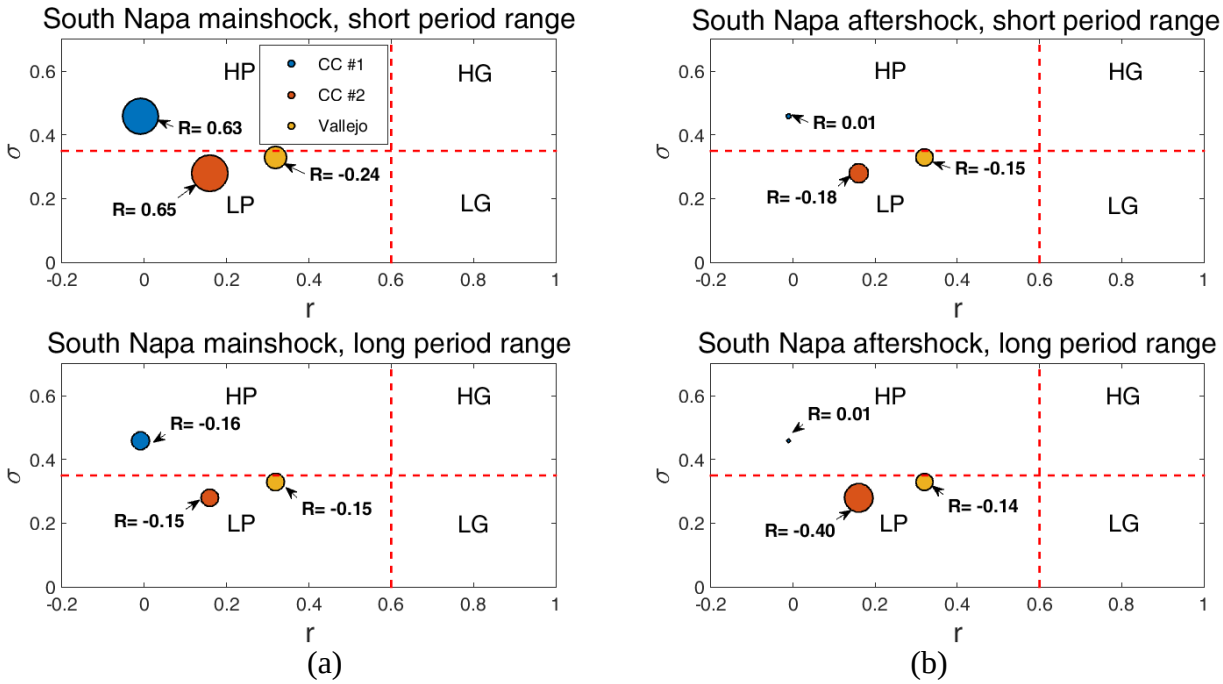

Figure 24. Correlation of taxonomy classes with spectral acceleration residuals at surface of MTH models for all three downhole arrays under the shaking of (a) South Napa Earthquake mainshock and (b) South Napa Earthquake aftershock

Conclusions

This paper evaluated the taxonomy class of three selected CSMIP downhole arrays with the recordings during the 2014 South Napa Earthquake. And the 1D SRA was performed in LS-DYNA for these arrays to study the effect of subsoil conditions on the amplification of ground motions. Both strong and weak shakings were analyzed for each array and the analysis results of the South Napa Earthquake mainshock and aftershock were discussed.

Overall, nonlinear finite element models for all arrays were capable of reproducing the ground motions very well over low frequency range (< 1 Hz) but failed to capture (in most cases

underestimated) the components of the motions intermediate and high frequencies (> 1 Hz). Besides, linear elastic models of arrays in general overestimated the soil response (especially for strong shaking case) and tended to yield intermediate period spectral acceleration peaks caused by resonance of soil profiles.

Regarding CC #1 and #2, GQH and MTH models well captured the soil responses at intermediate depths of soil profiles throughout a wide period range. However, they were unable to reproduce the large amplification of ground motions at surfaces, especially for short period range. These observations suggest that the amplifications of the ground motions at these 2 arrays were significantly influenced by 3D effects (surface waves, basin edge) and possibly structural response with surface waves emanating from the foundations.

As for Vallejo, the predictions of GQH and MTH models agreed fairly well with the observations at both surface and 17.9 m depth. It is noteworthy prominent overprediction was achieved for NS component instead of EW component between 0.2 sec to 0.4 sec for both strong and weak events. This could be attributed to nonhomogenous and anisotropic soil properties (spatial heterogeneity) at the site, which 1D SRA was unable to reproduce.

The strengths and limitations inherent in the practical application of 1D SRA model demonstrates the following: (i) 1D SRA is appropriate for sites with constantly layered stratigraphy in lateral directions, (ii) 1D SRA fails to account for 2D and 3D effects including spatial heterogeneity, nonvertical incidence, basin effects and topographic effects. Considering the presence of complex geologic and topographic conditions, 1D SRA is not quite effective or accurate in estimating site amplification in the selected downhole arrays, especially at shorter periods and large strains, which is consistent with the implications of taxonomy evaluation. As a means to understand the complexity of site response and the validity of 1D SRA assumptions, it is recommended to evaluate taxonomy class of a specific site prior to performing 1D SRA in engineering practice.

Acknowledgements

This project is funded by California Strong Motion Instrumentation Program, California Geological Survey. This support is gratefully acknowledged. We also thank Hamid Haddadi and Moh Huang for providing the needed information to undertake this research. We greatly appreciate Abbas Abghari and Caltrans for providing PS suspension logging data of CC #1 and Vallejo as well as geotechnical reports of all three downhole arrays studied in this paper.

References

Afshari, K., and Stewart, J. P. (2015). Effectiveness of 1D ground response analyses at predicting site response at California vertical array sites. *Proceedings of SMIP 15 Seminar on Utilization of Strong-Motion Data, October 22, 2015, pp. 23 – 40.*

Bray, J., Cohen-Waeber, J., Dawson, T., Kishida, T., and Sitar, N. (2014). Geotechnical engineering reconnaissance of the August 24, 2014 M6 South Napa earthquake. *Geotechnical Extreme Events Reconnaissance (GEER) Association Report Number GEER, 37.*

California Engineering Strong Motion Database (CESMD). *www.strongmotioncenter.org*.

Çelebi, M., Ghahari, S. F., & Taciroglu, E. (2015). Unusual Downhole and Surface Free‐Field Records Near the Carquinez Strait Bridges during the 24 August 2014 Mw 6.0 South Napa, California, Earthquake. *Seismological Research Letters*, 86(4), 1128-1134.

Groholski, D. R., Hashash, Y. M., Kim, B., Musgrove, M., Harmon, J., and Stewart, J. P. (2016). Simplified Model for Small-Strain Nonlinearity and Strength in 1D Seismic Site Response Analysis. *Journal of Geotechnical and Geoenvironmental Engineering, 04016042.*

Hashash, Y.M., Groholski, D.R., Phillips, C.A., Park D., and Musgrove M. *DEEPSOIL 6.1*, User Manual and Tutorial. Univ. of Illinois at Urbana-Champaign: Champaign, Illinois, 2016.

Kramer, S. L. (1996). *Geotechnical Earthquake Engineering*, Prentice Hall, Englewood Cliffs, New Jersey.

LSTC, 2012. LS DYNA Keyword User's Manual Volumes I & II – Release 971 R.6.1.0. Livermore Software Technology Corporation, Livermore, California.

Masing, G. Eigenspannungen und verfestigung beim messing. *In Proceedings of the 2nd international congress of applied mechanics (Vol. 100, pp. 332-5). sn.*

MATLAB, V. (2015). 8.5. 0.197613 (R2015a). The MathWorks Inc., Natick, Massachusetts.

Motamed, R., Stanton, K., Almufti, I., Ellison, K., & Willford, M. (2016). Improved Approach for Modeling Nonlinear Site Response of Highly Strained Soils: Case Study of the Service Hall Array in Japan. *Earthquake Spectra*, 32(2), 1055-1074.

Shakal, A., Haddadi, H., Huang, M., and Stephens, C. (2014). Highlights of Strong−Motion Data from the M6.0 South Napa Earthquake of August 24, 2014. *Proceedings of SMIP 14 Seminar on Utilization of Strong-Motion Data, October 9, 2014, pp. 111– 130.*

Stewart, J. P., Kwok, A. O., Hashash, Y. M. A., Matasovic, N., Pyke, R., Wang, Z., & Yang, Z. (2008). Benchmarking of nonlinear seismic ground response analysis procedures. *Rpt. No. PEER-2008, 4.*

Thompson, E. M., Baise, L. G., Tanaka, Y., & Kayen, R. E. (2012). A taxonomy of site response complexity. *Soil Dynamics and Earthquake Engineering, 41*, 32-43.